

# A New Method for Simulation of On-Chip Interconnects and Substrate Currents with 3D Alternating-Direction-Implicit (ADI) Maxwell Solver

Xi Shao<sup>1,2</sup>, Neil Goldsman<sup>2</sup>, Omar Ramahi<sup>2,3</sup>, Parvez N. Guzdar<sup>4</sup>

<sup>1</sup>Space Physics Data Facility, Goddard Space Flight Center, NASA, Greenbelt, MD 20171, USA

<sup>2</sup>Electrical and Computer Engineering Department, <sup>3</sup>Mechanical Engineering Department, <sup>4</sup>Institute for Research in Electronic and Applied Physics, University of Maryland, College Park, MD 20742, USA

Email: [shao@mail630.gsfc.nasa.gov](mailto:shao@mail630.gsfc.nasa.gov), [neil@eng.umd.edu](mailto:neil@eng.umd.edu), [oramahi@calce.umd.edu](mailto:oramahi@calce.umd.edu), [guzdar@ipr.umd.edu](mailto:guzdar@ipr.umd.edu)

**Abstract— We introduce a time-domain method to simulate the digital signal propagation along on-chip interconnects by solving Maxwell’s equations with the Alternating-Direction-Implicit (ADI) method. With this method, we are able to resolve the large scale (i.e. on-chip electromagnetic wave propagation) and fine scale (i.e. skin depth and substrate current) structure in the same simulation, and the simulation time step is not limited by the Courant condition. The simulations allow us to calculate in detail parasitic current flow inside the substrate; propagation losses; skin-depth; and dispersion of digital signals on non-ideal interconnects. We have found considerable substrate currents and losses that depend on the substrate doping.**

## I. INTRODUCTION

Inductive, capacitive coupling, and resistive losses in interconnects and substrates are significant barriers in the development of high-speed digital and analog IC’s. Accurate modeling of modern on-chip interconnects (including coupling and losses) usually requires a full-wave solution to Maxwell’s equations. However, such a solution is difficult because the wavelengths of interest are much larger than the fine topological structure of IC’s. (Wavelengths are typically on the mm to cm scale, while chip structures are on the micron scale.) In addition, digital and mixed (broadband) signal applications often require analysis in the time domain. Conventional Maxwell solvers typically use the explicit Finite-Difference-Time-Domain (FDTD) method. However, the conventional method is limited by the Courant condition ( $\Delta t < 1/\sqrt{c^2(1/\Delta x^2 + 1/\Delta y^2 + 1/\Delta z^2)}$ ), which requires prohibitively small time steps to resolve fine structure on the submicron scale. To overcome this problem, we have applied the Alternating-Direction-Implicit (ADI) method [1, 2], to solve Maxwell’s Equation in IC’s, and have overcome the Courant’s limit. We have used the method to model the Metal-Insulator-Semiconductor-Substrate (MISS) structure. The simulations allow us to calculate in detail parasitic current flow inside the substrate, propagation losses, skin-depth and dispersion of digital signals on non-ideal interconnects. We

have found considerable substrate currents and losses that depend on the substrate doping.

## II. SIMULATION METHOD

In the ADI method [1, 2], Maxwell’s equations (1) are discretized on the conventional Yee’s [3] staggered grids with the electric field on the grid cell edge center, and magnetic field on the grid cell face center. In this way, the zero-divergence of the magnetic field is maintained throughout the simulation.

$$\begin{aligned}\frac{\partial \vec{D}}{\partial t} &= \nabla \times \vec{H} - \vec{J}, \\ \frac{\partial \vec{B}}{\partial t} &= -\nabla \times \vec{E}, \\ \vec{B} &= \mu \vec{H}, \vec{D} = \epsilon \vec{E}, \vec{J} = \sigma \vec{E}\end{aligned}\quad (1)$$

At each step, by manipulating Maxwell’s equations, we transform the differential equations to a system of tri-diagonal algebraic equations. Here, we give an example of discretizing the  $E_x$  component (equations (2-7)) during the two alternating steps. In step 1, the first half ( $B_z$ ) of the right hand side in equation (2) and the first half ( $E_x$ ) of the right hand side in equation (3) are treated as implicit. We substitute equation (3) ( $B_{z,(i+1/2,j\pm 1/2,k)}^{n+1}$ ) back to equation (2) and obtain the tri-diagonal equation (4). For the other two dimensions ( $E_y$  and  $E_z$ ), we perform similar manipulation to form a system of tri-diagonal equations, which can be easily solved with a tri-diagonal matrix solver. The magnetic field is updated using equations similar to equation (3).

In the next step, we treat the other half ( $B_y$ ) implicit in equation (5), and ( $E_x$ ) as implicit in equation (6). We obtain the tri-diagonal system in equation (7) for  $E_x$ . Similarly, we can obtain the other two tri-diagonal systems for  $E_y$  and  $E_z$  and solve them to update the electric field. The magnetic field is updated with equations similar to equation (6).

These two steps are alternated thereafter. The detailed algorithm of ADI method can be found in [1, 2].

This work is supported by AFOSR and LPS.

STEP 1 (for  $E_x$  and  $B_z$  component):

$$\frac{\mathcal{E}E_{x,(i+1/2,j,k)}^{n+1} - \mathcal{E}E_{x,(i+1/2,j,k)}^n}{\Delta t} = \frac{1}{\mu} \frac{B_{z,(i+1/2,j+1/2,k)}^{n+1} - B_{z,(i+1/2,j-1/2,k)}^{n+1}}{\Delta y} - \frac{1}{\mu} \frac{B_{y,(i+1/2,j,k+1/2)}^n - B_{y,(i+1/2,j,k-1/2)}^n}{\Delta z} - \sigma E_{x,(i+1/2,j,k)}^{n+1} \quad (2)$$

$$\frac{B_{z,(i+1/2,j-1/2,k)}^{n+1} - B_{z,(i+1/2,j-1/2,k)}^n}{\Delta t} = \frac{E_{x,(i+1/2,j,k)}^{n+1} - E_{x,(i+1/2,j-1,k)}^{n+1}}{\Delta y} - \frac{E_{y,(i+1,j-1/2,k)}^n - E_{y,(i,j-1/2,k)}^n}{\Delta x} \quad (3)$$

$$a \times E_{x,(i+1/2,j-1,k)}^{n+1} + b \times E_{x,(i+1/2,j,k)}^{n+1} + c \times E_{x,(i+1/2,j+1,k)}^{n+1} = d, \text{ where}$$

$$a = -\frac{1}{\epsilon\mu} \frac{\Delta t^2}{\Delta y^2}$$

$$b = 1 + \frac{2}{\epsilon\mu} \frac{\Delta t^2}{\Delta y^2} + \frac{\Delta t}{\epsilon} \sigma$$

$$c = -\frac{1}{\epsilon\mu} \frac{\Delta t^2}{\Delta y^2}$$

$$d = E_{x,(i+1/2,j,k)}^n - \frac{1}{\epsilon\mu} \frac{\Delta t}{\Delta z} (B_{y,(i+1/2,j,k+1/2)}^n - B_{y,(i+1/2,j,k-1/2)}^n) + \frac{1}{\epsilon\mu} \frac{\Delta t}{\Delta y} (B_{z,(i+1/2,j+1/2,k)}^n - B_{z,(i+1/2,j-1/2,k)}^n) + \frac{1}{\epsilon\mu} \frac{\Delta t^2}{\Delta y} \left( -\frac{E_{y,(i+1,j+1/2,k)}^n - E_{y,(i,j+1/2,k)}^n}{\Delta x} + \frac{E_{y,(i+1,j-1/2,k)}^n - E_{y,(i,j-1/2,k)}^n}{\Delta x} \right) \quad (4)$$

STEP 2 (for  $E_x$  and  $B_y$  component):

$$\frac{\mathcal{E}E_{x,(i+1/2,j,k)}^{n+2} - \mathcal{E}E_{x,(i+1/2,j,k)}^{n+2}}{\Delta t} = \frac{1}{\mu} \frac{B_{z,(i+1/2,j+1/2,k)}^{n+1} - B_{z,(i+1/2,j-1/2,k)}^{n+1}}{\Delta y} - \frac{1}{\mu} \frac{B_{y,(i+1/2,j,k+1/2)}^{n+2} - B_{y,(i+1/2,j,k-1/2)}^{n+2}}{\Delta z} - \sigma E_{x,(i+1/2,j,k)}^{n+2} \quad (5)$$

$$\frac{B_{y,(i+1/2,j,k+1/2)}^{n+2} - B_{y,(i+1/2,j,k+1/2)}^{n+2}}{\Delta t} = \frac{E_{z,(i+1/2,j,k+1/2)}^{n+1} - E_{z,(i,j,k+1/2)}^{n+1}}{\Delta x} - \frac{E_{x,(i+1/2,j,k+1)}^{n+2} - E_{x,(i+1/2,j,k)}^{n+2}}{\Delta z} \quad (6)$$

$$a \times E_{x,(i+1/2,j,k-1)}^{n+2} + b \times E_{x,(i+1/2,j,k)}^{n+2} + c \times E_{x,(i+1/2,j,k+1)}^{n+2} = d, \text{ where}$$

$$a = -\frac{1}{\epsilon\mu} \frac{\Delta t^2}{\Delta z^2}$$

$$b = 1 + \frac{2}{\epsilon\mu} \frac{\Delta t^2}{\Delta z^2} + \frac{\Delta t}{\epsilon} \sigma$$

$$c = -\frac{1}{\epsilon\mu} \frac{\Delta t^2}{\Delta z^2}$$

$$d = E_{x,(i+1/2,j,k)}^{n+1} + \frac{1}{\epsilon\mu} \frac{\Delta t}{\Delta y} (B_{z,(i+1/2,j+1/2,k)}^{n+1} - B_{z,(i+1/2,j-1/2,k)}^{n+1}) - \frac{1}{\epsilon\mu} \frac{\Delta t}{\Delta z} (B_{y,(i+1/2,j,k+1/2)}^{n+1} - B_{y,(i+1/2,j,k-1/2)}^{n+1}) + \frac{1}{\epsilon\mu} \frac{\Delta t^2}{\Delta z} \left( \frac{E_{z,(i+1,j,k+1/2)}^{n+1} - E_{z,(i,j,k+1/2)}^{n+1}}{\Delta x} - \frac{E_{z,(i+1,j,k-1/2)}^{n+1} - E_{z,(i,j,k-1/2)}^{n+1}}{\Delta x} \right) \quad (7)$$

[1, 2, 4] show that the 3D-ADI method for solving Maxwell's equations is unconditionally stable, and the simulation time step is not limited by Courant's condition. In our code, the grid spacing is non-uniform in all three dimensions. This allows us to place enough resolution at the places of interest. The simulation time step is chosen to be able to resolve the band width of the signal. Mur's [5] first order absorption boundary condition is applied to simulate free space.

### III. MODEL VERIFICATION

To test the code we applied it to a standard metal skin depth problem with a known analytical solution. We performed a 2D simulation of EM wave propagation under a metal strip of conductivity =  $3.9 \times 10^7$  S/m. The domain bottom is bounded with Perfect Electric Conductor (PEC). The smallest grid size of 0.1  $\mu$ m is placed inside the metal. The grid along Z direction is of uniform size = 150  $\mu$ m. The Courant condition requires  $\Delta t < 0.33 \times 10^{-15}$  sec. Our simulation time step is  $\Delta t = 2 \times 10^{-13}$  sec. The excitation frequency = 50 GHz. The skin current  $\mathbf{J}_z$  inside the metal has the analytical solution

$$\mathbf{J}_z \propto \cos(k_z z + y / \delta) \times \exp(-y / \delta), \quad (8)$$

$\delta$  is the skin depth =  $\sqrt{2 / (\omega\mu\sigma)}$  and  $k_z$  is the wave number along the guide. Inside the metal, the wave is damped in the Y direction and grazes along the Z direction. Fig. 1b shows the agreement between the simulation and analytical calculation for current  $\mathbf{J}_z$  inside the metal. The agreement is excellent. With the ADI method, we are able to reveal the grazing wave pattern inside the metal.

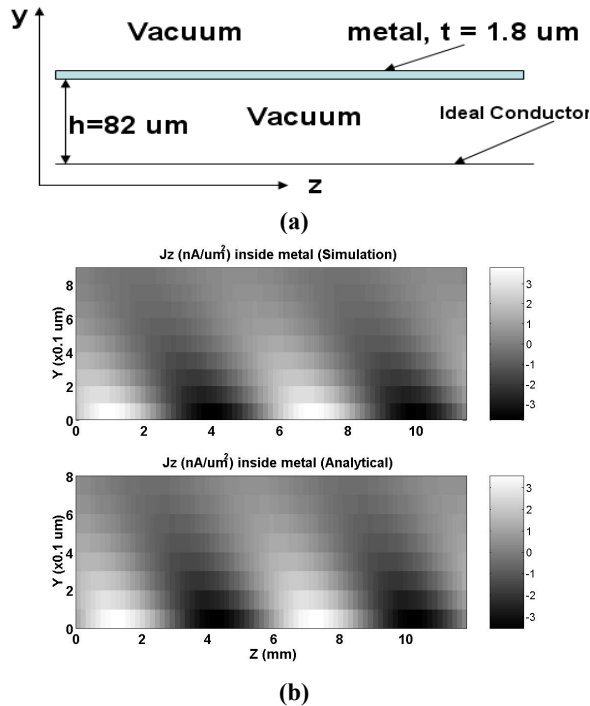


**Figure 1:** Model Verification: shows excellent agreement between numerical and analytical result. (a) Geometry. Source at  $z = 0$ ;  $f = 50$  GHz. (b) pattern of the current  $\mathbf{Jz}$  inside the metal obtained from the simulation and analytical calculation. The metal strip conductivity =  $3.9 \times 10^7$  S/m.

#### IV. SIMULATION RESULTS

We applied the 3D ADI code to study the digital pulse propagation along Metal-Insulator-Semiconductor-Substrate (MISS) structure. Fig. 2 shows a cross-section of the interconnect MISS structure we simulated with our ADI code. Along  $Z$ , the direction of wave propagation, we have 120 grid

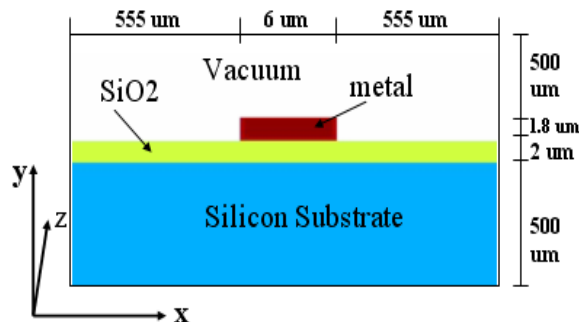


**Figure 2:** Cross section of the simulated MISS structure. The XY cross section of the metal strip is  $6 \mu\text{m} \times 1.8 \mu\text{m}$  and thickness of the  $\text{SiO}_2$  layer is  $2 \mu\text{m}$ .  $Z$  is the direction of propagation and lumped current flow.

points of uniform spacing =  $25 \mu\text{m}$ . In XY cross-section we have a non-uniform mesh with finest grid spacing =  $0.1 \mu\text{m}$ ; and the time step is  $\Delta t = 1 \times 10^{-13}$  sec, giving  $83 \times 89 \times 120$  space grid points, with 1000 time steps. The simulation time is 3-4 hours on a PC.

Fig. 3 shows simulation results for a fast 1V, 20psec digital pulse of rise-time = 2ps, excited at one end of the interconnect. The metal strip conductivity =  $5.8 \times 10^7$  S/m, typical for copper. The substrate doping is set to be  $n = 10^{17} / \text{cm}^3$ , which corresponds to substrate conductivity = 2260 S/m. Fig. 3a shows the voltage signal at  $Z = 0, 500$ , and  $1000 \mu\text{m}$ . At  $Z = 500$  and  $1000 \mu\text{m}$ , the signal amplitude is lowered and broadened. The higher frequency components of the signal suffer larger damping. Figure 3b shows cross section of  $\mathbf{E}_y$  at  $Z = 1000 \mu\text{m}$  and  $t = 50$  ps. The  $\mathbf{E}_y$  field concentrates inside the  $\text{SiO}_2$  layer. This corresponds to the skin-depth mode propagation along the MISS structure [6]. The EM field is guided along the channel formed by the metal skin current and substrate current. Figures 3c shows the XY-cross section of current  $\mathbf{Jz}$  inside the metal (along the direction of the signal propagation), at  $Z = 1000 \mu\text{m}$  and  $t = 37$  ps. We see that due to the skin depth effect, the current concentrates near the metal edges and surfaces, giving rise to resistive losses. Figure 3d shows the top view of substrate current  $\mathbf{Jz}$  at  $5 \mu\text{m}$  below the  $\text{SiO}_2$  layer for  $t = 37$  ps. The bright and dark shaded areas correspond to the rising and falling of the signal, showing the spread of the current almost a tenth of a  $\text{mm}$  away from the interconnect edge, which can obviously lead to parasitic cross talk. Fig. 3e shows side view giving the depth of the substrate current. The substrate skin depth is tens of microns. The substrate current contributes most to the parasitic interconnect losses.

Fig. 4 shows the voltage at different  $Z$  locations for substrate doping changing from  $n = 10^{16}$  and  $10^{18} / \text{cm}^3$ . The EM waves, all of which are in the skin-depth mode region [6], suffers different dispersion and dissipation for different substrate dopings. Lower substrate doping in this region yields more losses and dispersion.

#### V. SUMMARY

In this paper, we show that the ADI method is efficient in simulating signal propagation along on-chip interconnects. We are able to study both the EM wave propagation and the detailed metal skin depth and substrate current effects without being limited by the Courant's condition.

#### REFERENCES

- [1] T. Namiki, A new FDTD algorithm based on alternating-direction-implicit method, IEEE Trans. Microwave Theory Tech., vol. 47, pp. 2003-2007, Oct., 1999.
- [2] F. Zheng, Z. Chen, and J. Zhang, A finite-difference time-domain method without the courant stability condition, IEEE Microwave Guided Wave Lett., Vol.9, pp. 441-443, Nov., 1999.
- [3] K. S. Yee, Numerical solution of initial boundary value problems involving Maxwell's equation in isotropic media, IEEE Trans. Antennas Propagat., vol. AP-14, pp.302-307, May 1966.
- [4] T. Namiki, 3-D ADI-FDTD method - Unconditionally stable time-domain algorithm for solving full vector Maxwell's equations, IEEE Trans. Microwave Theory Tech., vol.48, pp. 1743, Oct., 2000.

[5] G. Mur, Absorbing boundary conditions for the finite-difference approximation of the time-domain electromagnetic field equations, IEEE Trans. Electromagn. Compat., EMC-23, pp. 377-382, Nov., 1981.  
 [6] T. Shibata, and E. Sano, Characterization of MIS structure coplanar transmission lines for investigation of signal propagation in integrated circuits, IEEE Trans. Microwave Theory Tech., vol. 38, pp. 881-890, Jul., 1990.

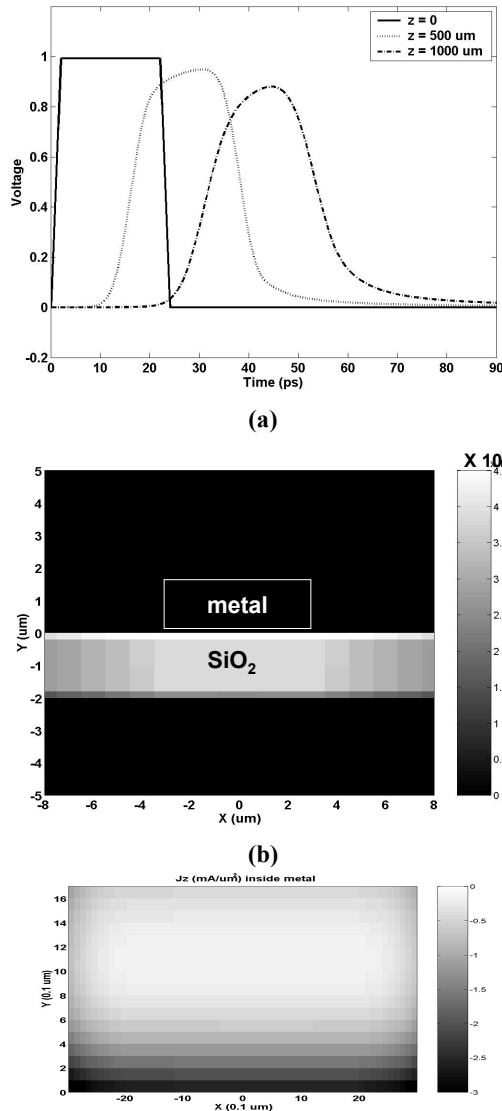


**Figure 3:** (a) Voltage observed at different Z locations ( $z=500$   $\mu\text{m}$ ,  $1000$   $\mu\text{m}$ ) along the MISS strip. Solid line shows simulation with substrate doping =  $10^{17}$  / $\text{cm}^3$ . Shows digital signal losses and dispersion. (b) Cross section of  $E_y$  (V/m) field at  $Z=1$ mm and  $t= 50$  ps. The dark shading corresponds to the weak electric field. The electric field  $E_y$  concentrates in the SiO<sub>2</sub> layer. (c) Cross section of current  $J_z$  (mA/ $\mu\text{m}^2$ ) inside the metal at  $Z=1$ mm and  $t= 37$  ps. The dark color corresponds to strong current. Shows metal skin-depth effect losses.

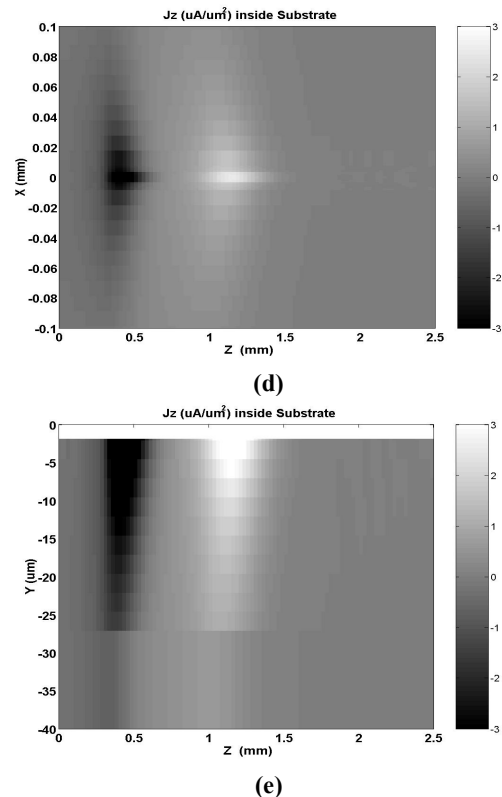


**Figure 3: (Continued)** (d) Top view of current  $J_z$  ( $\mu\text{A}/\mu\text{m}^2$ ) in the substrate ( $5\mu\text{m}$  below SiO<sub>2</sub> layer) at  $t = 37$  ps. Bright and dark shaded areas correspond to the rising and falling of the signal. Shows potential interference and coupling in lateral direction. (e) Side view of current  $J_z$  ( $\mu\text{A}/\mu\text{m}^2$ ) in substrate at  $X = 0$ . Shows current penetration to the substrate. Substrate doping  $n = 10^{17}$  / $\text{cm}^3$ .

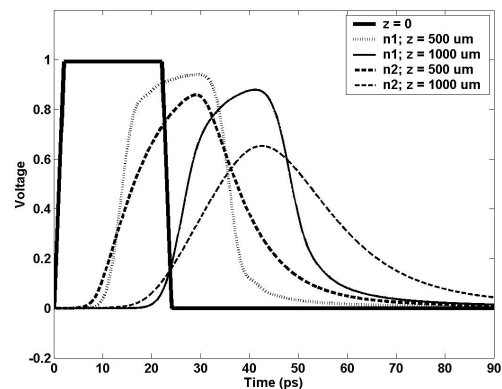


**Figure 4:** Voltage observed at different Z locations along the MISS strip with substrate doping  $n1 = 10^{18}$ , and  $n2 = 10^{16}$  / $\text{cm}^3$ .